AIAA JOURNAL
Vol. 46, No. 7, July 2008

OH-Planar Fluorescence Measurements of Pressurized, Hydrogen Premixed Flames in the SimVal Combustor

P. A. Strakey* and S. D. Woodruff†
National Energy Technology Laboratory, Morgantown, West Virginia 26507
and
T. C. Williams‡ and R. W. Schefer§
Sandia National Laboratories, Livermore, California 94551

DOI: 10.2514/1.32640

Planar laser-induced fluorescence measurements of the hydroxyl radical in lean, premixed natural gas flames augmented with hydrogen are presented. The experiments were conducted in the Simulation Validation combustor at the National Energy Technology Laboratory at operating pressures from 1 to 8 atmospheres. The data, which were collected in a combustor with well-controlled boundary conditions, are intended to be used for validating computational fluid dynamics models under conditions directly relevant to land-based gas turbine engines. The images, which show significant effects of hydrogen on local flame quenching, are discussed in terms of a turbulent premixed combustion regime and nondimensional parameters such as Karlovitz number. Pressure was found to thin the OH region, but only had a secondary effect on overall flame shape compared with the effects of hydrogen addition, which was found to decrease local quenching and shorten the turbulent flame brush. A method to process the individual images based on local gradients of fluorescence intensity is proposed, and results are presented. Finally, the results of several large eddy simulations are presented and compared with the experimental data in an effort to understand the issues related to model validation, especially for simulations that do not include OH as an intermediate species.

I. Introduction

THE goals of the U.S. Department of Energy Turbines Program require the flexibility to produce clean, efficient power with fuels that contain high concentrations of hydrogen. These goals include a NOx emission target of 2 ppm by volume at firing temperatures that are roughly the same or higher than the current state-of-the-art gas turbine engines. One of the issues involved in hydrogen combustion is the significantly higher flame speed of hydrogen relative to methane. The ability to design and field a fuel-flexible, low emissions combustor will depend largely upon the understanding of fundamental combustion processes that govern such phenomenon as turbulent premixed flame propagation, flashback, and NOx formation. It is also expected that computational fluid dynamics (CFD), including large eddy simulation (LES), will play a significant role in the development of a fuel-flexible combustor. There is, however, a serious lack of experimental data related to lean-premixed hydrogen combustion, especially at pressures relevant to gas turbine combustor operating conditions. The goal of this study is to provide detailed experimental data for CFD model validation as well as fundamental combustion knowledge using the National Energy Technology Laboratory (NETL) Simulation Validation (SimVal) combustor. The SimVal combustor is a high-pressure, optically accessible can-style combustor using swirl stabilization that was specifically designed for the purposes of generating model validation data using laser-based diagnostic techniques such as OH-planar laser-induced fluorescence (OH-PLIF).

OH-PLIF is one of the most common combustion diagnostics for several reasons. First, it is a two-dimensional technique that provides data for a slice through the flowfield and provides some indication about spatial structures within the flame. Secondly, it is a relatively easy technique to apply compared with more complex diagnostics like coherent anti-Stokes Raman spectroscopy (CARS) or Raman scattering. Importantly, OH-PLIF data can be used to identify the flame front, which is a key piece of information for the purposes of validating CFD combustion models.

The use of OH-PLIF as an indicator of the flame front or heat release is complicated by the relatively long lifetime of the OH radical in the post-flame region. In nonpremixed flames, OH usually only exists in a thin layer near the stoichiometric mixture fraction and makes identification of the flame front straightforward. In premixed flames, OH, which is rapidly produced in the flame front, is gradually consumed in the post-flame region through radical recombination reactions. CH, another intermediate species, has a much shorter lifetime and can be more easily related to heat release. The difficulty in applying CH-PLIF is the significantly lower concentrations of CH in lean-premixed flames, especially with hydrogen enriched flames. The fundamentals of laser-induced fluorescence, including the OH molecule in particular, have been described in detail previously [1].

Hedman et al. have made extensive use of OH-PLIF to characterize lean-premixed natural gas/air flames in a laboratory-scale gas turbine combustor developed at Wright–Patterson Air Force Base [2]. They studied the effects of equivalence ratio and swirler geometry on flame structure, looking at both the mean OH concentration field and the instantaneous fields, noting the wide variation in flame structure in the instantaneous images.

Presented as Paper 980 at the 45th AIAA Aerospace Sciences Meeting and Exhibit, Reno, NV, 8–11 January 2007; received 5 June 2007; revision received 19 December 2007; accepted for publication 3 January 2008.

*Research Scientist, Energy Systems Dynamics Division, 3610 Collins Ferry Road, Post Office Box 880; pstrakey@netl.doe.gov.
†Research Scientist, Energy Systems Dynamics Division, 3610 Collins Ferry Road, Post Office Box 880.
‡Postdoctoral Fellow, Hydrogen and Combustion Technologies, Post Office Box 969.
§Technical Staff, Hydrogen and Combustion Technologies, Post Office Box 969.

The shot-to-shot variation in flame structure was believed to be due to the strongly swirling and recirculating flow in the combustor.

Donbar et al. applied OH-PLIF imaging in a hydrocarbon-fueled scramjet combustor to ascertain the effects of fuel type, combustor operating conditions, and degree of premixing on flame anchoring and the large-scale flame structure [3]. The data obtained provided a fundamental understating of where the flame was anchoring in the combustor as well as where local extinction was taking place. They also observed an effect of pressure oscillations on the combustion process at supersonic conditions. They demonstrated the value of information that can be obtained by using a time-resolved, two-dimensional technique such as OH-PLIF imaging.

OH-PLIF was used to study the effects of hydrogen enrichment on a lean-premixed methane flame with hydrogen addition at concentrations in the fuel up to 20% [4]. Flame stability and lean extinction were investigated using a swirl-stabilized premixing nozzle similar to what was used in the present study but conducted in an unconfined combustor at atmospheric pressure. The addition of hydrogen extended the lean stability margin and also greatly increased the OH concentration at any given equivalence ratio. Furthermore, there was a significant decrease in OH concentration as the equivalence ratio was decreased, and the occurrence of "gaps" in the OH images corresponding to flame quenching occurred more frequently at lower equivalence ratios.

A combination of OH and CH-PLIF in a lean, swirl-stabilized, nonpremixed model combustor operating on methane and air was applied by Weigand et al. [5] Their results demonstrated the superiority of CH over OH imaging as an indicator of flame front but noted that significant CH mole fractions were only found at the richer conditions studied, and, even then, the signals were typically 500 times less than the OH signal.

Simultaneous OH-PLIF and planar Rayleigh temperature imaging in an industrial-scale, lean-premixed, swirl-stabilized combustor at atmospheric pressure was reported by Dinkelacker et al. [6] The technique identified various regimes of combustion including flameletlike burning, thickened flame regions and even local flame quenching. Having simultaneous temperature measurements allowed the determination of whether an area lacking in OH was either unburned reactants or recirculated combustion products that had lower levels of OH. By calculating the gradient of OH on the leading edge of the flame and comparing this to laminar flame calculations, the extent of flame stretch or thickening was determined. A similar study conducted with a wire stabilized flame [7] showed that turbulent flame stretching could be related to the Karlovitz number, $Ka = (\delta_L/\eta_0)$, which is defined here as the ratio of the laminar flame thickness to the Kolmogorov turbulence microscale. The Karlovitz number was varied by changing the stoichiometry.

OH-PLIF has been applied as a standard method of characterizing flame structure along with various other methods such as particle image velocimetry (PIV) by Griebel et al. [8] Most of this work was conducted in a pressurized dump combustor using grid-generated turbulence without swirl. OH-PLIF data were collected at pressures up to 10 bars, and an increase in flame wrinkling was observed due to the increase in Reynolds number and Karlovitz number as pressure and gas density were increased. No significant effects of pressure on flame-front location was observed.

Almost all of the published works using OH-PLIF to characterize turbulent flames have been qualitative in nature, meaning that the fluorescence signal is assumed to be a linear function of OH concentration, but no attempt is made to calibrate the system to provide absolute OH concentration values. The main reason for this is the relative difficulty involved in system calibration, which must be done under conditions similar to that in the actual combustion device. Arnold et al. [9] did describe (in an unpublished work) a process for system calibration using a flat flame burner in a pressurized chamber. They showed that it is possible to calibrate for a known temperature and concentration field. They also observed a significant decrease in fluorescence signal with increasing pressure due to collisional quenching or deactivation of the excited OH molecule.

To calibrate and correct for collisional quenching in a complex combustor flowfield, the local temperature and species concentrations must be known, which would involve a complex diagnostic campaign. Lastly, it is largely recognized that even relative OH measurements can provide invaluable data on flame-front location and structure as a function of combustor geometry and operating conditions.

The purpose of this study is to provide detailed combustion data, largely for the purpose of validating CFD combustion models, under conditions relevant to industrial gas turbines, which typically operate at pressures up to about 30 bars with preheated air. This paper is the first such effort at NETL to characterize OH concentration in an optically accessible swirl-stabilized combustor typical of gas turbine can-style combustors at pressures up to 8 bars using blends of natural gas and hydrogen as a fuel.

II. Experimental Approach

The SimVal research combustor was designed as a test bed for generating data for validating CFD models such as combusting LES. The test facility consists of the following major components: the optically accessible research combustor; an optically accessible test section; natural-gas, hydrogen, and air flow loops; and a gas sampling system. In the current test configuration, the facility can provide a maximum combustion air flow rate of 1.23 kg/s, a maximum natural gas flow rate of 53.3 g/s, a maximum hydrogen flow rate of 2.3 g/s, a maximum combustion air preheat temperature of 810 K, and a maximum combustor internal pressure of 2.31 MPa. The geometry of the combustor and pressure chamber is shown in Fig. 1.

Optical access through the test section is available through four 17.8 cm wide by 30.5 cm high viewports. Optical access through the combustor outer liner is available through four equally spaced 10.2 cm wide by 30.5 cm high windows, which are aligned with the test section viewports. The combustor inner liner is a quartz tube with a length of 31.8 cm and an internal diameter of 18.0 cm, which is representative of the tube diameter of can-style combustors and the dome height of annular combustors. The metal components of the combustor are backside water cooled, and the heat fluxes through these components are calculated based on the measured water flow rates and temperature rises. Although the quartz liner is not actively cooled, significant heat losses occur here as well because of radiative cooling. Estimations of heat loss through the liner have been previously made through infrared imaging of the temperature of the inner and outer surfaces of the liner [10]. Characterization of the heat losses is critical for application of this data to model validation.

The approach flow supplied to the swirler is fully premixed and spatially uniform. This is accomplished in the current combustor configuration by installing an inlet choke plate 12.7 mm upstream of the leading face of the swirler. The plate chokes the flow of premixed fuel and air by restricting the flow to ~1320 laser-drilled, 0.43 mm holes, which are evenly distributed across the annulus. In this

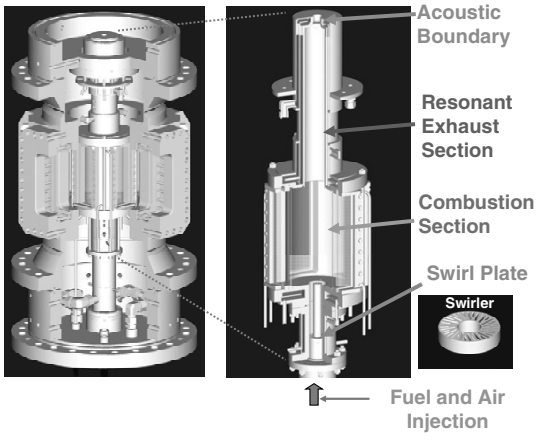

Fig. 1 Schematic of the combustor test section and pressure chamber.

baseline configuration (and unlike a conventional fuel–air premixer), fuel is injected into the combustion airstream upstream of the swirler through eight radial fuel injection spokes, which are arrayed in a single plane 25.7 cm upstream of the inlet choke plate. This approach produces a spatially uniform flow immediately above the choke plane, isolates the flow acoustically from upstream processes and hardware, and assures full premixing of the fuel–air mixture. This was confirmed by CFD modeling of the mixing process, which indicated that the fuel and air were well mixed before the swirl plate.

For the tests reported here, the exhaust choke shown in Fig. 1 was removed to allow independent control of combustor pressure and inlet velocity. The combustor pressure was controlled with a backpressure valve. Further details of the combustor and test facility can be found elsewhere [11]. The natural gas used in this study was sampled daily for content and had a typical composition of 96.0% CH_4, 2.5% C_2H_6, 0.4% C_3H_8, and 0.7% N_2, with the balance being higher hydrocarbons. The equivalence ratios reported here are calculated based on the measured carbon-to-hydrogen ratio in the natural gas plus the added hydrogen.

The combustor produces the classical "tulip-shaped" flame with an inner recirculation zone (IRZ) and a corner recirculation zone (CRZ) characteristic of common swirl-stabilized combustors. The test conditions presented here encompassed pressures ranging from 1 to 8 atmospheres, preheat temperatures of 520 to 600 K, hydrogen concentration in the fuel of 0 to 60%, and an equivalence ratio of 0.6.

The OH-PLIF system consisted of a Quanta-Ray DCR-2A Nd:YAG laser, PDL-1 dye laser, and doubling crystal to produce ~10 ns laser pulses at 10 Hz with about 6 mJ of output per pulse at the Q1(9) line of the (1, 0) band of the OH $A^2\Sigma - X^2\Pi$ electronic transition at 283.92 nm. This particular line was selected because it is one of the strongest transitions and has only a mild temperature dependence over the ranges of temperatures expected here. The line location was determined by scanning the dye laser through a Bunsen flame and comparing the resulting spectrum to calculations performed with the LIFBASE code [12].

The dye laser had a specified full-width half-maximum line width of 0.2 cm^{-1}, which translated to a line width of 0.3 cm^{-1} after frequency doubling. The line width of the OH transition was estimated using the LIFBASE code, including pressure broadening effects, and is shown in Fig. 2 along with the calculated laser profile. Because the Q2(8) transition overlaps the Q1(9) transition, especially at high pressure, it is likely that excitation of both lines was achieved. At atmospheric pressure the laser line is clearly wider than the OH transition, and the overlap integral is roughly 70%. At a pressure of 8 bars, the overlap is nearly 100%, which should serve to increase the fluorescence signal as pressure increases.

A combination of fused silica cylindrical and spherical lenses was used to form a laser sheet approximately 125 mm high and 200 μm thick, which was directed through the center of the combustor. At the

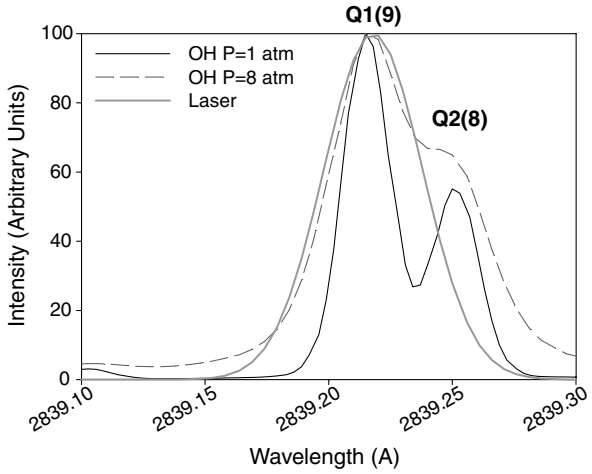

Fig. 2 Estimated laser spectral profile along with simulated OH profiles at 1 and 8 bars using the LIFBASE code.

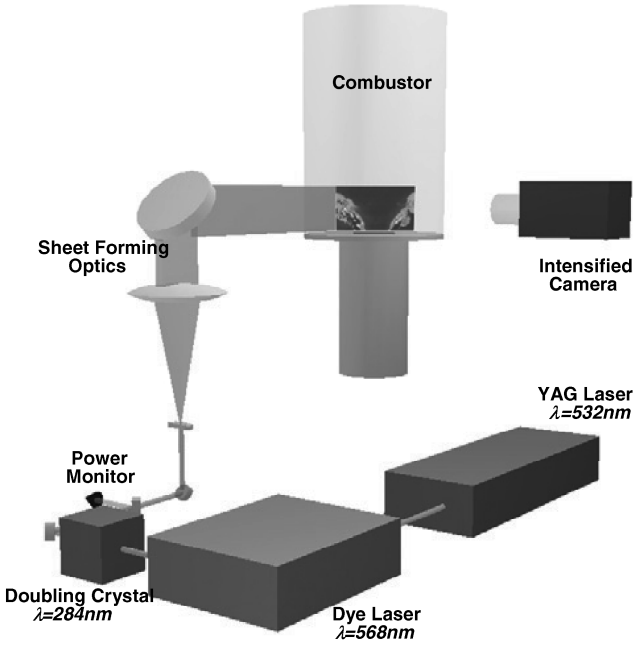

Fig. 3 Diagram of the OH-PLIF optical setup.

laser power density used here, the OH absorption should be well into the linear regime, far from saturation. A schematic of the setup is provided in Fig. 3. A Princeton Instruments I-Pentamax intensified camera with a 512 × 512 sensor and a 45 mm f1.8 fused silica lens with both longpass and bandpass filters was used to image the fluorescence signal around 310 nm while blocking most of the unwanted scattered laser light. The filed of view was 117 mm square, which yielded a resolution of 229 mm per pixel.

The total average laser power before and after the combustor was monitored using two photodiodes observing diffuse reflections of the laser beam and a boxcar integrator to average the signals. The average input laser power was found to vary only slightly over the course of the experiments. The nonuniform intensity distribution of the laser sheet was determined before the experiment by imaging the fluorescence from a well-mixed, acetone doped nitrogen flow passing through the combustor under cold-flow conditions. The OH fluorescence images were corrected for the laser sheet intensity variation by normalizing the images against the acetone image.

III. Results and Discussion

Table 1 provides some measured and calculated quantities covering the extent of the test conditions. The turbulent fluctuating velocity, u', was taken as the average value at the dump plane measured under cold-flow conditions at a similar inlet velocity using particle image velocimetry [13]. The assumption here is that u' is independent of fuel type and operating pressure. Note that the bulk inlet velocity was held constant at 40 m/s for all of the data presented here. The integral length scale l was estimated to be equal to the width of the slots in the swirler. The kinematic viscosity is based on the preheat temperature, and the rest of the quantities are calculated values. Laminar flame speed was calculated using the GRI3.0 mechanism. To better understand what regimes of turbulent premixed combustion were encountered in this study, the Borghi diagram for turbulent premixed combustion is plotted in Fig. 4, along with our calculated data points at 1 and 8 bars for both fuel compositions. Keeping in mind that the turbulence parameters are only inlet flow approximations, it appears that for the pure natural gas fuel, we might expect to encounter a range of combustion regimes because the data points fall very close to the border between the thickened flame regime and the well-stirred reactor regime. Adding hydrogen to the fuel decreases the Karlovitz number and pushes the combustion down into the thickened flame regime.

Table 1 Summary of fuel properties and characteristic conditions for the range of test conditions

	0% H_2 $P = 1$ bar	0% H_2 $P = 8$ bars	60% H_2 $P = 1$ bar	60% H_2 $P = 8$ bars
Natural gas in fuel, %	100	100	40	40
Equivalence ratio, ϕ	0.6	0.6	0.6	0.6
Preheat temperature T, in K	530	580	530	580
Adiabatic flame temperature T_{ad}, in K	1845	1875	1895	1925
Turbulent fluctuating velocity u', m/s	30	30	30	30
Turbulent integral length scale (estimated) l, mm	2.5	2.5	2.5	2.5
Kinematic viscosity (inflow) ν, m^2/s	4.0e − 5	5.0e − 6	4.0e − 5	5.0e − 6
Turbulent Reynolds number $Re_l = u' \cdot l/\nu$	1905	15,240	1905	15,240
Kolmogorov scale $\eta_0 = l \cdot Re_l^{-0.75}$, μm	9.0	1.9	9.0	1.9
Laminar flame speed S_L, m/s	0.63	0.21	0.99	0.34
Laminar flame thickness (Zeldovich) $\delta_L = \nu/S_L$, μm	63.5	23.8	40.4	14.7
Karlovitz number $Ka = (\delta_L/\eta_0)$	7.1	12.5	4.5	7.7

All of the images presented here have been corrected for the variation in laser sheet intensity distribution in the vertical direction, and the location of the centerbody and annulus is annotated on the bottom of the figures.

A. Effect of Hydrogen

Figure 5 contains a series of three instantaneous images of OH fluorescence intensity at atmospheric pressure for the baseline (100% natural gas) fuel. In each image, the location of the centerbody and annulus is annotated at the bottom of the images. The cold reactant jet can be identified by the lack of any OH fluorescence in the region just downstream of the annulus. The shear layer between the cold reactant jet and the hot recirculating combustion products is where the flame is anchored and most of the heat release takes place. This region can be identified in the images by the high fluorescence intensity indicating superequilibrium levels of OH (intensity > 5000 counts). Downstream of the flame zone, the OH concentration relaxes back down to the equilibrium level through a series of recombination reactions. This region dominates the majority of the field of view with a nearly continuous "blue background" (~3000 counts) in the images. The background noise, which was determined by tuning the dye laser away from the OH absorption line, was found to be much lower than the signals shown in the images. The dark streak near the top of the images was due to a defect in the outer liner window.

One-dimensional laminar flame calculations of OH mole fraction are presented in Fig. 6 for both fuels and at pressures of 1 and 4 bars. In the figure, the flow is from left to right. The steep gradient at the leading edge of the flame is a clear indicator of the presence of combustion, and the OH follows a trend similar to what was observed in the images.

Although the flame does appear to be anchored on the tip of the centerbody, combustion here appears to be only intermittent, with most of the heat release occurring much farther downstream near the tip of the flame brush, which is outside of the field of view in these experiments. The combustion chamber is 180 mm in diameter, and so the images in Fig. 5 represent about 65% of the width of the

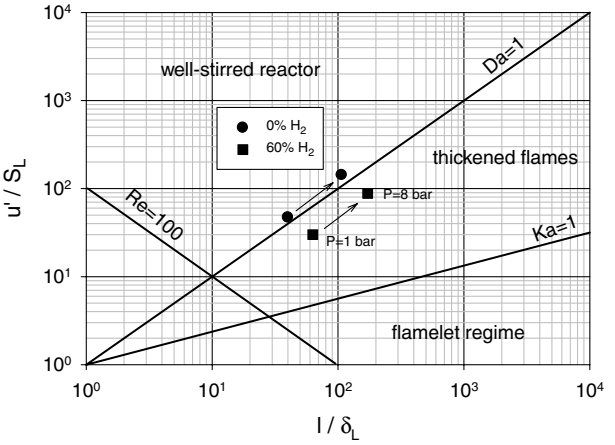

Fig. 4 Borghi turbulent premixed combustion diagram with current estimated operating points plotted for both fuels at 1 and 8 bars.

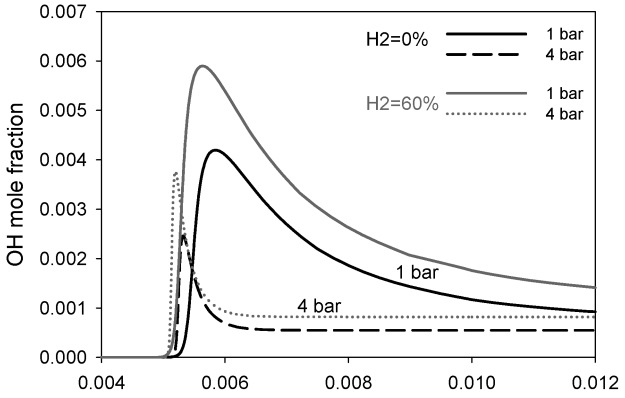

Fig. 6 Premixed unstretched laminar flame calculations of OH profiles through the flame for both fuels at pressures of 1 and 4 bars. Calculated using the GRI3.0 mechanism.

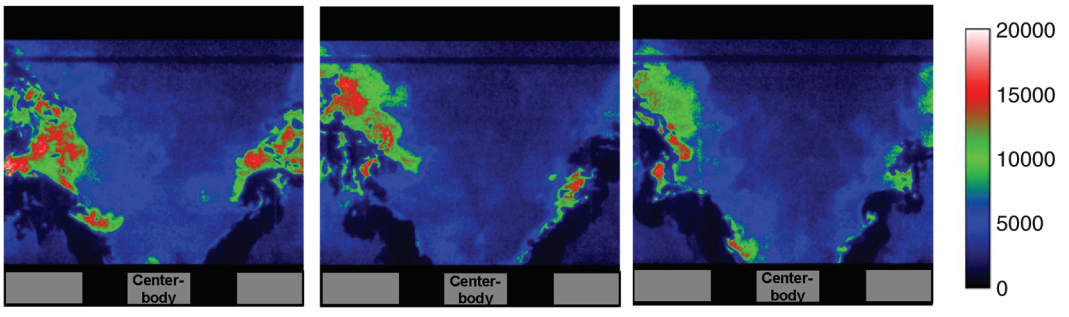

Fig. 5 Three instantaneous snapshots of OH fluorescence for 0% hydrogen flame at an operating pressure of 1 bar.

combustor. The fact that there does not appear to be a continuous flame sheet for the natural gas fuel indicates that significant flame quenching may be occurring. Dinkelacker et al. [6] made simultaneous two-dimensional OH-PLIF and temperature measurements in a similar combustion environment and observed similar quenching effects. They showed that the equilibrium background of OH was at a temperature close to the burned gas temperature and that the regions where equilibrium levels of OH were in contact with the cold reactant core without producing superequilibrium levels of OH were regions where the flame was stretched beyond the critical limit, and quenching of the flame occurred. Similar regions were observed here near the dump plane in Fig. 5, where the velocity gradients in the shear layer were very high. Dinkelacker et al. noted that flame stretch and quenching were increased as the Karlovitz number increased due to a decrease in equivalence ratio. This is consistent with the estimation of combustion regime plotted in the Borghi diagram in Fig. 4.

Adding hydrogen to the fuel significantly enhanced combustion near the tip of the centerbody and greatly shortened the length of the unburned reactant core, also referred to as the flame brush length as shown in Fig. 7. The flame is now able to anchor in the inner shear region near the centerbody. This is consistent with the increase in laminar flame speed and decrease in Karlovitz number for the 60% hydrogen fuel (see Table 1). Some quenching does still occur in the outer shear layer. The outer shear layer, which is in contact with the combustion products in the CRZ, is quenched due to the substantial heat losses in the CRZ, which is in contact with the water-cooled dump plane. CFD simulations have indicated that the temperature in the CRZ is several hundred degrees less than the temperature in the IRZ. With the addition of hydrogen (Fig. 7), the faster reaction kinetics are able to overcome the heat losses, and some degree of combustion can be seen to occur in the outer shear layer.

The addition of hydrogen also resulted in a thinner, more compact OH region with significantly more combustion occurring very near the dump plane. This can be explained by the faster reaction kinetics of hydrogen compared with methane. The laminar flame-speed for the 60% hydrogen fuel was estimated to be about 57% higher than the pure natural gas fuel. With the addition of hydrogen, the corresponding decrease in Karlovitz number and susceptibility to flame quenching resulted in a shorter flame brush. Also note that with the addition of hydrogen, the flame is anchoring farther out into the annulus, away from the centerbody, which seems to imply that combustion might be occurring further upstream into the premixing nozzle. This is also a result of the faster reaction kinetics and flame speed of hydrogen and implies an increased potential for flashback with hydrogen-based fuels.

The cold reactant core in Fig. 7 is more difficult to identify because of the presence of background noise in the images. As mentioned earlier, tuning the dye laser away from the OH transition line resulted in a background image with very low intensity relative to the images in Fig. 7, and so the background noise is not suspected to be scattered laser light leaking through the camera filters. One possibility is secondary fluorescence from OH outside of the laser sheet due to absorption and reemission of the fluorescence signal at 310 nm. Because the spontaneous fluorescence within the laser sheet emanates in all directions, much of this can be absorbed by OH in the combustion gasses in front of and behind the laser sheet, which would produce a background "glow" all throughout the combustor. This effect was further implied by measurements of laser power after the combustor, which indicated that roughly 25% of the laser light was being absorbed by OH, even at atmospheric pressure, indicating that the environment within the combustor is not optically thin. The fact that the problem is worse for the 60% hydrogen fuel could be a result of the higher equilibrium levels of OH as shown in Fig. 6.

The effect of hydrogen on flame quenching can be seen somewhat more easily in Fig. 8, which contains the averaged OH fluorescence images for both fuels at 1 bar. Each image in Fig. 8 is the average of 200 instantaneous images, and the average images were rescaled so that the maximum fluorescence intensity was equal to the maximum display scale. For the baseline fuel, combustion is only occurring in the inner shear layer between the cold reactants and hot combustion products in the IRZ, as was identified in the instantaneous images. The increase in combustion in the outer shear layer with the addition of hydrogen is again observed, and this would also contribute to the shortening of the flame brush length that can be seen in the figure.

B. Effect of Pressure

Figure 9 shows a series of three instantaneous images of OH fluorescence intensity at a pressure of 8 bars for the 60% hydrogen fuel. These images can be compared with the images in Fig. 7, which are for the 60% hydrogen fuel at 1 bar, noting that the images in Fig. 9 were rescaled for purposes of clarity. Thinning of the OH region is

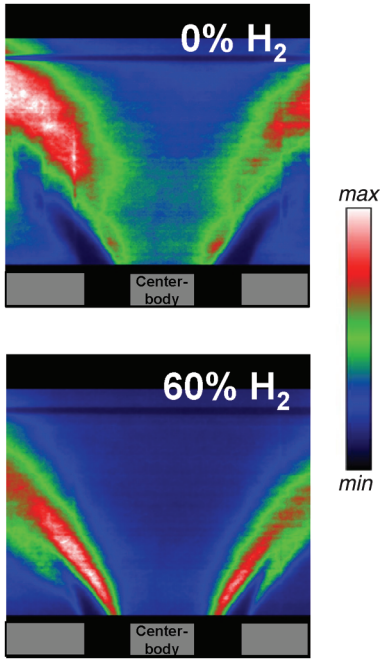

Fig. 8 Average OH fluorescence images (from 200 instantaneous images) for the baseline fuel (top) and the 60% hydrogen fuel (bottom) at an operating pressure of 1 bar.

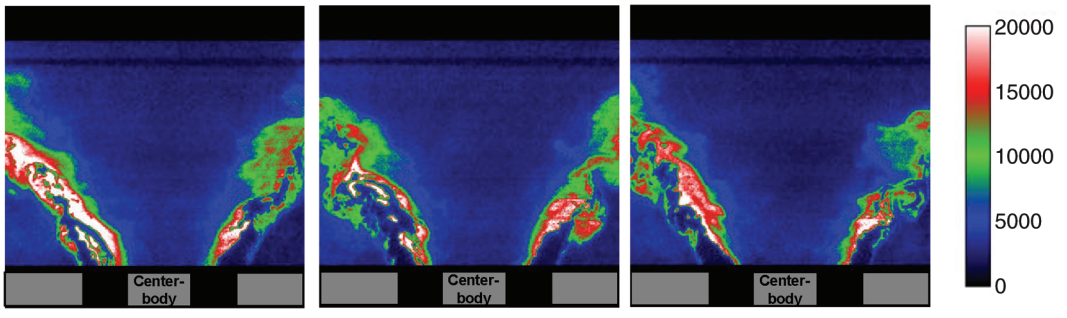

Fig. 7 Three instantaneous snapshots of OH fluorescence for 60% hydrogen flame at an operating pressure of 1 bar.

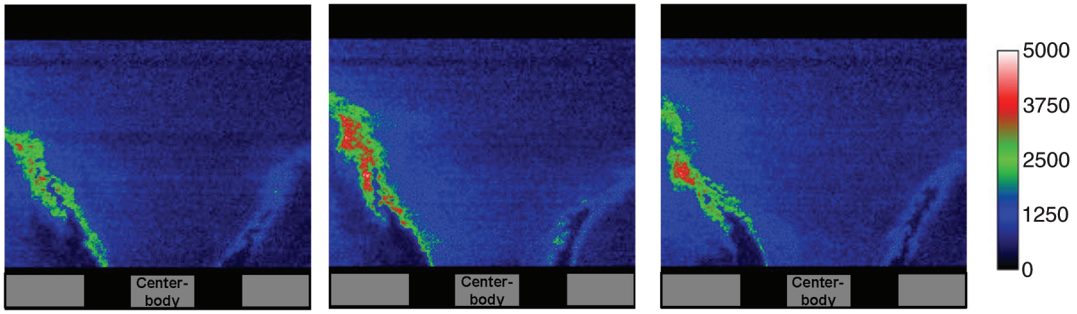

Fig. 9 Three instantaneous snapshots of OH fluorescence for the 60% hydrogen flame at an operating pressure of 8 bars.

evident in Fig. 9, as pressure is increased from 1 to 8 bars, which is consistent with the laminar premixed flame calculations shown in Fig. 6 and is a result of three-body recombination reactions depleting the OH concentration more rapidly at higher pressures. Attenuation of the laser sheet (from left to right), although negligible at 1 bar, becomes severe at 8 bars due to the increase in absolute OH concentration. Although correction of the images for laser sheet attenuation may be possible for the averaged images assuming that the images are bilaterally symmetric, it is not possible for the instantaneous images.

The average peak fluorescence intensity was found to be inversely proportional to pressure, even though the absolute OH concentration increased roughly with $p^{0.67}$. The pressure dependence on OH concentration is a result of the linear increase in gas density with pressure and the decrease in OH mole fraction with increasing pressure as shown in Fig. 6. Analysis of the instantaneous images, however, showed that the peak fluorescence intensity scaled with $p^{-0.63}$.

This pressure dependence is mainly due to collisional deactivation of the excited OH molecules. For laser-induced fluorescence in the linear regime, with spontaneous emission lifetimes much longer than the collisional quenching lifetime, the fluorescence signal is inversely proportional to the collisional quenching rate. For OH at atmospheric pressure, the spontaneous lifetime, determined from the Einstein coefficient, is on the order of several hundred nanoseconds. Typically, OH fluorescence signals decay within a few nanoseconds, indicating that collisional quenching is indeed the most important determining factor in OH fluorescence signal intensity [14]. The collisional quenching rate is expressed as $Q = \sum k_i \cdot n_i$, where k_i are the species and temperature-dependent quenching cross sections, and n_i are the species number densities [15]. A first-order quenching analysis, assuming that species mole fractions and temperature are independent of pressure, indicates that collisional deactivation should scale with number density (i.e., pressure) squared. Combining this effect with the absolute increase in OH concentration yields a fluorescence signal that is proportional to $p^{-1.3}$. The fact that the observed pressure dependence on fluorescence signal was weaker here was due to several reasons.

As was mentioned earlier, as operating pressure was increased, the OH linewidths increased due to pressure broadening (Fig. 2), which increased the overlap integral with the laser line. A second effect is an increase in combustor temperature with operating pressure. Analysis of the wall heat losses in the combustor, which was determined by the measured water temperatures and flow rates, showed that the combustor heat losses, relative to the sensible heat input, decreased from 13 to 4% as pressure was increased from 1 to 8 bars. This was also confirmed by the measured temperature in the exhaust section, which increased from 1580 to 1820 K as pressure was increased from 1 to 8 bars for the baseline fuel. The increase in combustor temperature with operating pressure would increase the peak OH mole fraction as well as slightly decrease the collisional quenching cross sections. These combined effects could explain the discrepancy between the observed pressure effect and the anticipated effect from quenching theory. Collisional quenching makes it very difficult to convert the relative fluorescence intensity into absolute OH concentration and explains why the vast majority of OH-PLIF studies report relative intensity rather than absolute OH concentration.

Another effect of increasing the operating pressure is to increases the Karlovitz number and thus the likelihood of flame quenching or local extinction. This can be seen in a qualitative sense in comparing the fluorescence intensity in the outer shear layer between Figs. 7 and 9. At 8 bars, there was somewhat less combustion occurring in the outer shear layer. This was mostly due to the decrease in laminar flame speed as pressure was increased. The effect of the heat losses was to increase the temperatures in the CRZ with increasing pressure, which should therefore increase the laminar flame speed slightly, but this cannot overcome the decrease in laminar flame speed with increasing pressure.

Average fluorescence images are provided in Fig. 10 for both fuels at all four operating pressures. Note that the images were not scaled equally and are provided to show the qualitative effects of fuel type and operating pressure.

C. Flame-Front Probability

The main goal of this study is to provide data for CFD validation, specifically LES models. Because most practical LES studies of gas turbine combustors involve mechanistic combustion subgrid models such as the G equation or progress variable approaches, or global one- or two-step finite-rate mechanisms, direct validation using OH concentration or fluorescence intensity is usually not possible. Although efforts are being made to provide detailed species and temperature measurements in model combustors at elevated pressures [16], the vast majority of efforts in validating LES codes are aimed at validation of the location of the flame front. The flame front can be identified from the OH-PLIF images as the steep gradients in fluorescence intensity at the leading edge of the flame.

To systematically extract flame-front locations from all of the images in a consistent manner, an image-processing algorithm was constructed to identify and mark the location of the flame front based on intensity gradients. The instantaneous images were converted into gradient images using a second-order central differencing scheme to calculate the intensity gradients in the x and y directions and then represent this as the magnitude of the gradient $I_g = \sqrt{I_{g,x}^2 + I_{g,y}^2}$. The flame front was discriminated from the trailing edge of the flame and general background noise using a threshold criteria. Values of the threshold between 25 and 50% of the maximum gradient in each image were found to provide good discrimination of the flame front. As the threshold is decreased, the flame brush increases somewhat, and this becomes a parameter that requires some judgment. An example of the image processing sequence is provided in Fig. 11, which shows an instantaneous image of fluorescence intensity with a subregion selected, followed by the gradient image, and finally the image after thresholding at 25%.

The binarized image in the right of Fig. 11, which represents the probability of flame presence, contains regions of flame assigned a value of 1 or regions without flame assigned a value of 0. The individual binarized images can then be ensemble averaged to produce two-dimensional maps of the probability density function (PDF) of flame location. The mean and root-mean squared PDFs of

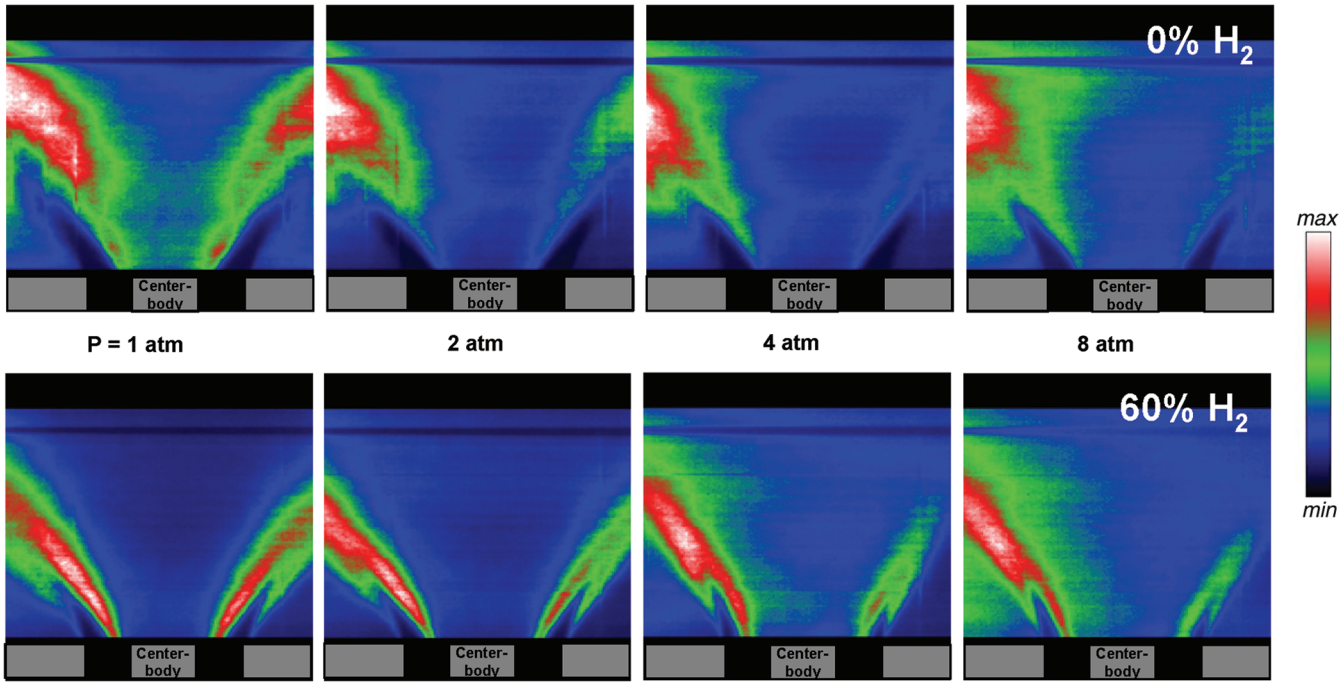

Fig. 10 Average OH fluorescence images for the baseline fuel (top row) and the 60% hydrogen fuel (bottom row) with operating pressure increasing from let to right.

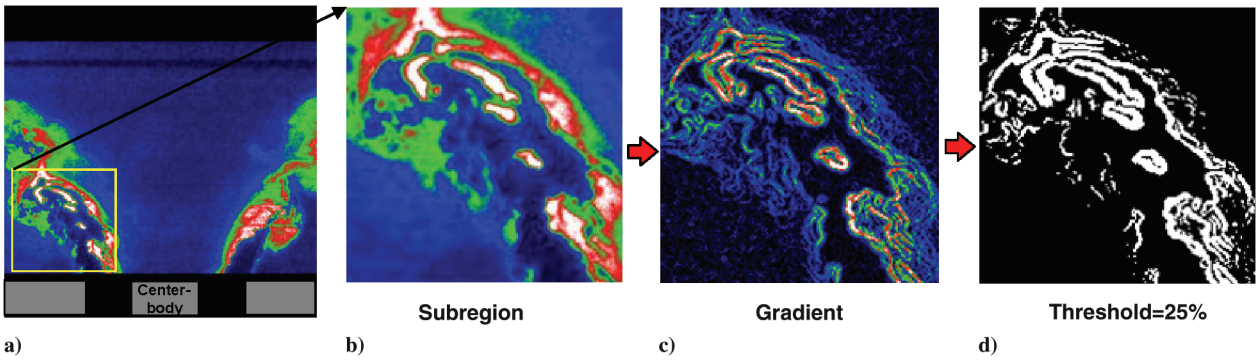

Fig. 11 Sequence of images from the image processing algorithm. a) Single image, b) subregion, c) gradient of intensity, d) clipped at 25% of maximum.

flame location can be directly compared with an LES result using, for instance, the location of the G isocontour or the gradient of progress variable. In processing the images, it was found that the attenuation of the laser sheet (from left to right) created a decrease in the intensity gradient and hence an artificially lower probability of flame on the right side of the images. It was decided to process only the left side of the images because the time-averaged flame shape was found to be bilaterally symmetric about the axis of the combustor.

Figure 12 contains the average PDF maps of flame location from the left half of the fluorescence images for each fuel at all four pressures. On each image, the left half of the image is with the baseline fuel, and the right half is with the 60% hydrogen fuel. Because the maximum intensity gradient changed with both fuel composition and pressure, the images were rescaled to a maximum PDF value of 1. It is therefore not possible to compare absolute flame probability between different operating pressures and fuels, only

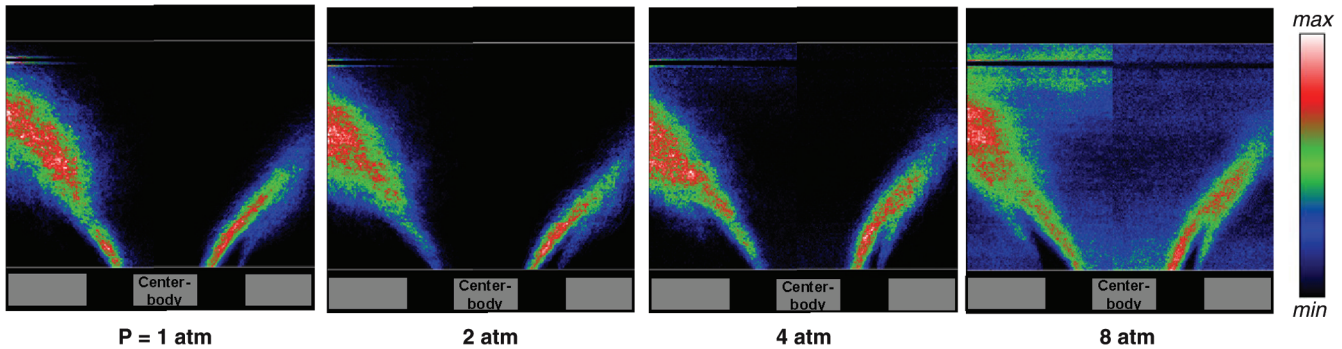

Fig. 12 Average probability contour maps of flame location for baseline fuel (left half of each image) and 60% hydrogen fuel (right half of each image). Pressure is increasing from left to right.

relative probability in space at any given condition. From the images, it is clear that the addition of hydrogen had a large impact on flame location, whereas operating pressure had only a minor impact. The background noise present across a large portion of the 8-bar PDF image in Fig. 12 is the result of noise in the original OH-PLIF image, which was due to the low fluorescence signal at this pressure and is not the result of combustion occurring in these regions. This noise could be reduced by the selection of a higher threshold criteria in the image processing sequence.

Radial profiles of the PDFs were extracted at axial locations of 10, 25, and 50 mm from the dump plane at pressures of 1 and 8 bars and are plotted in Fig. 13. As with the images in Fig. 12, the left half of each plot is for the baseline fuel, and the right half is for the 60% hydrogen fuel.

D. Validation Test

In an effort to determine the applicability of the present approach of using OH-PLIF imaging for validating combustion codes, a series of LES simulations were performed with the current combustor geometry. The code used here was Fluent 6.2, which is a commercial finite-volume-based CFD code with a broad range of modeling capabilities. The three-dimensional computational domain encompassed the 360 deg region from the exit of the swirl plate downstream to 9 cm into the exhaust section and was composed of approximately 1.2 million hexahedral cells with a small layer of tetrahedral cells near the face of the swirl plate. The grid was partitioned into 16 blocks, and calculations were performed on a Linux cluster.

The individual slots at the entrance to the domain were modeled as mass flow inlets with specified axial and tangential velocity components corresponding to a 30 deg flow angle. The mass flow rate was fixed at 0.045 kg/s, which corresponded to the atmospheric pressure case. The exit in the exhaust section was modeled as a pressure outlet and the simulations were run as incompressible.

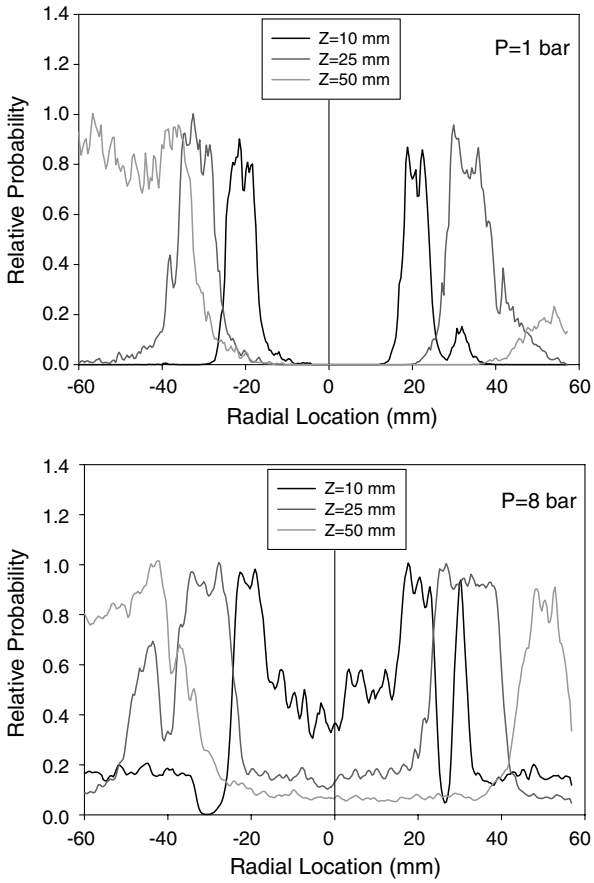

Fig. 13 Radial profiles of flame PDF extracted from the images in Fig. 12 for axial locations of 10, 25, and 50 mm from the dump plane at pressure of 1 bar (top plot) and 8 bars (bottom plot). Left half of each plot is for the 0% hydrogen fuel and right half is for the 60% hydrogen fuel.

The subgrid viscosity model used here was the dynamic Smagorinski model [17], and the discretization scheme used for the momentum equation was a second-order accurate bounded central differencing scheme in space and a second-order backward differencing scheme for the temporal discretization. The bounded central differencing scheme uses pure central differencing by default, but reverts to a blend of central differencing and upwinding schemes when the convection boundedness criteria is violated. The scalar equations were discretized with a second-order upwind scheme.

Two combustion modeling approaches were taken here. The first was the progress variable approach [18] in which the combustion source term was derived from the turbulent flame speed, which was calculated from an empirical correlation based on the subgrid turbulent kinetic energy. The progress variable is a conserved scalar that represents the degree of combustion. A value of zero is assigned to the unburned gas and a value of 1 to the burned gas. This approach only requires the inclusion of one additional transport equation over a noncombusting simulation and is computationally inexpensive and commonly used in LES combustion simulations. The second combustion modeling approach was a finite-rate chemistry approach ignoring subgrid turbulence chemistry interaction. This is equivalent to the assumption of infinitely fast mixing of the subgrid scalars. The kinetic mechanism was a 5-step, 9-species augmented reduced mechanism, which included OH and CO as intermediate species and was derived from the GRI2.1 mechanism for methane combustion [19]. This mechanism has been validated against the GRI2.1 mechanism over a fairly wide range of lean equivalence ratios and pressure up to 20 bars. This mechanism was chosen because it includes OH and thus can be directly compared with the experimental OH fluorescence images. Also, because it only includes nine species, it is computationally tractable using in situ adaptive tabulation to speed up the calculation of the reaction source terms [20]. Overall, this approach was found to be about three times more computationally expensive than the progress variable approach.

For both simulations, the water-cooled walls of the combustor were set at a fixed temperature of 400 K, which was found to provide roughly the correct amount of heat losses compared to the experimentally measured heat losses. Gas-phase radiation was also included using the discrete ordinates approach, with a weighted sum of gray gasses model for the emissivities of H_2O and CO_2. The quartz liner was modeled as a radiation boundary, and heat losses through the liner were verified to be close to experimental values derived from infrared imaging of the liner temperature.

The time step used was 5 μs for both simulations, which corresponded to a maximum Courant–Friedrichs–Lewy (CFL) number of 2 near the inlet and about 0.25 in the nozzle section. The simulations were run for about 60 ms, which corresponded to about 15 flow-through times of the nozzle section. This was found to be adequate to obtain good statistical quantities in the combustion region.

Figure 14 contains a comparison between the average OH-PLIF image (from Fig. 8) on the left half of the figure and the time-averaged OH mole fraction contour plot from the LES simulation over an equivalent field of view in the combustor in the right half of the figure. The time-averaged OH mole fraction from the LES simulation was computed by simply averaging the OH field at each time step over the course of about 10,000 time steps, or 40 ms of physical time, which was found to be adequate in achieving a "steady-state" time-averaged condition. The scale is again provided for relative comparison of OH concentration. The comparison between experiment and simulation is relatively good, especially considering the simplistic combustion approach and likely underresolution of the grid. The simulation did show a shorter unburned reactant core, and this is likely due to the assumption of infinitely fast mixing in the subgrid scale. Also, the LES grid is believed to be underresolved based on the estimated Taylor microscale, which could lead to excessive numerical dissipation and an increased sensitivity to the subgrid modeling approach. No

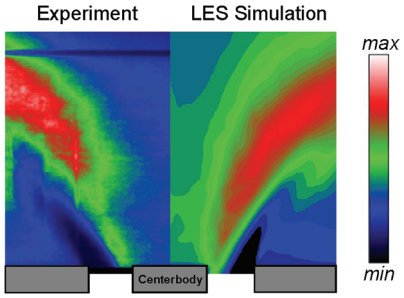

Fig. 14 Average OH fluorescence intensity (left half) from experiment using the baseline fuel at 1 bar and the result of the finite-rate chemistry LES simulation (right half) showing ensemble averaged OH mole fraction over the same viewing region.

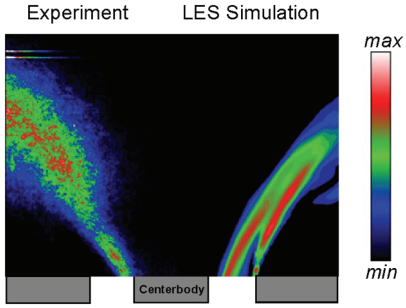

Fig. 15 Average OH gradient clipped at 25% (left half) from experiment using the baseline fuel at 1 bar and the result of the progress variable LES simulation (right half) showing ensemble averaged rate of formation of progress variable over the same viewing region.

attempt was made to refine the grid, as the purpose here is not to identify shortfalls of the modeling approach but to demonstrate the applicability of the validation approach using the raw OH-PLIF images.

The second validation comparison, shown in Fig. 15, is for the progress variable modeling approach. Because this model does not include intermediate species such as OH, the OH gradient method discussed in the previous section was used to validate against the rate of formation of progresses variable from the simulation. The rate of formation of the progress variable is essentially an overall reaction rate or fuel consumption rate, which laminar flame calculations have shown to occur in the leading edge of the flame where the OH gradients are the steepest. In Fig. 15, the ensemble averaged gradient image after thresholding at 25% of the maximum gradient is shown in the left half of the figure, and the ensemble averaged rate of formation of the progress variable from the simulation is shown in the right half of the image. The progress variable approach resulted in a less favorable comparison with the experimental data. One issue is the inability of this modeling approach to account for heat loss effects on the laminar and turbulent flame speeds. This resulted in combustion occurring in the CRZ and the outer shear layer, whereas the experimental results clearly show that combustion is quenched in this region. A secondary effect related to this is the shorter flame brush predicted by the model. The example does, however, demonstrate the ability to use the OH gradient method to validate CFD simulations that do not explicitly calculate OH concentration.

IV. Conclusions

Measurements of planar laser-induced fluorescence of the hydroxyl radical in lean, premixed natural gas flames augmented with hydrogen were presented over a range of pressures from 1 to 8 bars. The addition of hydrogen to the natural gas fuel was found to have a significant impact on local flame quenching and the length of the turbulent flame brush. Local flame quenching, which was found to be occur over large regions of both the inner and outer shear layers for the natural gas fuel, was substantially decreased with the addition of hydrogen. This was attributed to the higher laminar flame speed of hydrogen relative to methane. Addition of hydrogen to the natural gas based fuel also resulted in the flame front moving farther upstream into the premixing nozzle and indicates a potential problem for flashback with high-hydrogen fuels.

Increasing the operating pressure was found to decrease the OH zone thickness, and OH fluorescence intensity was also found to be inversely proportional to pressure to the 0.63 power due to collisional quenching of the excited OH molecule. Some increase in local flame quenching was also observed as pressure was increased. This was attributed to the decrease in laminar flame speed with increasing pressure.

Whereas direct study of the raw OH-PLIF images was found to be useful in understanding combustion phenomenon, for purposes of model validation, an image processing method was developed based on the magnitude of the OH fluorescence gradient. To discriminate the leading edge of the flame front from the trailing edge and background noise, a threshold criteria was applied to the gradient images to identify the flame front and the mean PDF maps of flame-front probability were presented.

Two examples of the application of this data to validate LES results were provided using two very different combustion modeling approaches within the LES simulations. The first approach, using semidetailed chemistry with the inclusion of the OH intermediate species, was found to be directly comparable to the raw OH-PLIF data. The second combustion modeling technique presented here, based on the progress variable approach, was found to be more relevant to the OH gradients extracted from the images using a threshold criteria. Whereas some discrepancies in flame structure were found between the simulations and the experimental data, the applicability and significance of the OH-PLIF validation techniques presented here were clearly demonstrated.

The data presented here are mainly for purposes of providing a fundamental physical understating of the effects of hydrogen addition on flame structure and for qualitative validation of computational models. Much of the data collected in this study was not presented here for the sake of brevity, but can be made available upon request to the authors. Current efforts are geared toward proving velocity data in the combustor from particle image velocimetry at the same conditions presented in this study.

Acknowledgments

The support of the U.S. Department of Energy Turbines Program is gratefully acknowledged. The authors would like to thank Todd Sidwell, Mark Tucker, and Mike Dera for their invaluable contributions in the operation of the combustor and the facility.

References

[1] Daily, J. W., "Laser Induced Fluorescence Spectroscopy in Flames,"*Progress in Energy and Combustion Science*, Vol. 23, 1997, pp. 133–199. doi:10.1016/S0360-1285(97)00008-7

[2] Hedman, P. O., Fletcher, T. H., Graham, S. G., Timothy, G. W., Flores D. V., and Haslam, J. K., "Observations of Flame Behavior in a Laboratory-Scale Premixed Natural Gas/Air Gas Turbine Combustor From PLIF Measurements of OH," *Proceeding of ASME Turbo Expo 2002*, GT-2002-30052, American Society of Mechanical Engineers, Fairfield, NJ, 2002.

[3] Donbar, J. M., Gruber, M. R., Jackson, T. A., Carter. C. D., and Mathur, T., "OH Planar Laser-Induced Fluorescence Imaging in a Hydrocarbon-Fueled Scramjet Combustor," *Proceedings of the Combustion Institute*, Vol. 28, 2000, pp. 679–687.

[4] Schefer, R. W., "Hydrogen Enrichment for Improved Lean Flame Stability," *International Journal of Hydrogen Energy*, Vol. 28, 2003, pp. 1131–1141. doi:10.1016/S0360-3199(02)00199-4

[5] Weigand, P., Meier, W., Dunn, X. R., Stricker, W., and Aigner, M., "Investigations of Swirl Flames in a Gas Turbine Model Combustor I. Flow Field, Structures, Temperatures, and Species Distributions," *Combustion and Flame*, Vol. 144, 2006, pp. 205–224. doi:10.1016/j.combustflame.2005.07.010

[6] Dinkelacker, F., Soika, A., Most, D., Hofmann, D., Leipertz, A., Polifke, W., and Dobbeling, K., "Structure of Locally Quenched Highly Turbulent Lean Premixed Flames," *27th Symposium (International) on Combustion*, Combustion Institute, Pittsburgh, PA, 1998, pp. 857–865.
[7] Soika, A., Dinkelacker, F., and Leipertz, A., "Measurement of the Resolved Flame Structure of Turbulent Premixed Flames with Constant Reynolds Number Bad Varied Stoichiometry," *27th Symposium (International) on Combustion*, Combustion Institute, Pittsburgh, PA, 1998, pp. 785–792.
[8] Griebel, P., Scharen, R., Siewert, P., Bombach, R., Inauen, A., and Kreutner, W., "Flow Field and Structure of Turbulent High-Pressure Premixed Methane/Air Flames," *Proceedings of ASME Turbo Expo 2003*, GT2003-38398, American Society of Mechanical Engineers, Fairfield, NJ, 2003.
[9] Arnold, A., Bombach, R., Kappeli, B., and Schlegel, A., "Quantitative Measurements of OH Radical Concentration Fields by Two-Dimensional Laser Induced Fluorescence," Paul Scherrer Institute, http://lpc.web.psi.ch/publications.html [retrieved 10 Oct. 2006] (unpublished).
[10] Beer, S. K., Woodruff, S. D., Dera, T. M., and Tucker, M. S., "Near-IR Imaging System for Measuring Temperatures in a Low-NOx Combustor," *Review of Scientific Instruments*, Vol. 77, 026103, 2006.
[11] Sidwell, T., Richards, G., Casleton, K., Straub, D., Maloney, D., Strakey, P., Ferguson, D., Beer, S., and Woodruff, S., "Optically Accessible Pressurized Research Combustor for Computational Fluid Dynamics Model Validation," *AIAA Journal*, Vol. 44, No. 3, March 2006, pp. 434–443. doi:10.2514/1.15197
[12] Luque, J., and Crosley, D. R., "LIFBASE: Database and Spectral Simulation (Version 1.5)," SRI International Rept. MP 99-009, 1999.
[13] Strakey, P., and Yip, J., "Experimental and Numerical Investigation of a Swirl Stabilized Premixed Combustor under Cold-Flow Conditions," *Journal of Fluids Engineering*, Vol. 129, 2007, pp. 942–953. doi:10.1115/1.2743665
[14] Kollner, M., Monkhouse, P., and Wolfrum, J., "Time-Resolved LIF of OH ($A^2\Sigma^+$, $v' = 1$ and $v' = 0$) in Atmospheric-Pressure Flames Using Picosecond Excitation," *Chemical Physics Letters*, Vol. 168, Nos. 3–4, May 1990, pp. 355–360. doi:10.1016/0009-2614(90)85624-L
[15] Tamura, M., Berg, P., Harrington, J., Luque, J., Jeffries, J., Smith, G., and Crosley, D., "Collisional Quenching of CH(A), OH(A), and NO(A) in Low Pressure Hydrocarbon Flames," *Combustion and Flame*, Vol. 114, 1998, pp. 502–514. doi:10.1016/S0010-2180(97)00324-6
[16] Wehr, L., Meier, W., Kutne, P., and Hassa, C., "Single-Pulse 1D Laser Raman Scattering Applied in a Gas Turbine Model Combustor at Elevated Pressure," *31th Symposium (International) on Combustion*, Combustion Institute, Philadelphia, PA, 2006, pp. 3099–3106.
[17] Kim, W., and Menon, S., "Application of the Localized Dynamic Subgrid-Scale Model to Turbulent Wall-Bounded Flows," *Presented at the 35th Aerospace Sciences Meeting*, AIAA Paper 97-0210, Jan. 1997.
[18] Zimont, V. L., and Lipatnikov, A. N., "A Numerical Model of Premixed Combustion of Gasses," *Chemical Physics Report*, Vol. 14, No. 7, 1995, pp. 993–1025.
[19] Mallampalli, H. P., and Fletcher, T. H., "Evaluation of CH_4/NOx Global Mechanisms Used for Modeling Lean Premixed Turbulent Combustion of Natural Gas," University of Southern California, Paper 96F-098, 1996.
[20] Pope, S. B., "Computationally Efficient Implementation of Combustion Chemistry Using In-Situ Adaptive Tabulation," *Combustion Theory and Modeling*, Vol. 1, 1997, pp. 41–63.

R. Lucht
Associate Editor